ARTICLE   OPEN

Check for updates

Poleward migration as global warming's possible self-regulator to restrain future western North Pacific Tropical Cyclone's intensification

I-I Lin [1] ✉, Suzana J. Camargo [2], Chun-Chi Lien [1], Chun-An Shi[1] and James P. Kossin[3,4]

Poleward migration is an interesting phenomenon regarding the shift of Tropical Cyclones (TCs) towards higher latitudes. As climate warms, TCs' intensification is promoted, and yet over certain oceans, TCs may also migrate poleward into colder waters. To what extent this poleward shift can impact future TC's intensification is unclear, and a quantitative understanding of these competing processes is lacking. Through investigating one of the most likely TC basins to experience poleward migration, the western North Pacific (WNP), here we explore the issue. Potential Intensity (PI, TC's intensification upper bound) along TC's intensification locations (from genesis to the lifetime maximum intensity location) are analysed. We find that poleward migration can partially cancel global warming's positive impact on future WNP TC's intensification. With poleward migration, the PI increasing trend slope is gentler. We estimate that poleward migration can reduce the increasing trend slope of the proportion of Category-5 PI by 42% (22%) under a strong (moderate) emission pathway; and 68% (30%) increasing trend slope reduction for the average PI.

INTRODUCTION

Tropical cyclones (TCs) are severe natural disasters. How TCs will change under anthropogenic climate change is of great concern[1–29]. As climate warms, it has been projected that TCs may move towards higher latitudes (poleward migration)[30–40], how poleward migration can impact future TC's intensification is therefore an important question to ask. Because poleward migration may involve different TC metrics, e.g., genesis location, lifetime maximum intensity (LMI) location, intensification track (genesis to LMI) or the entire TC track[30–40], this research focus on the intensification track.

As TCs move towards higher latitudes, one would naturally anticipate that poleward migration could negatively impact future TC's intensification, since TCs are also shifting towards a colder (less favourable) ocean environment as climate warms. Nevertheless, how to quantify this impact is a complex issue. Though high-resolution climate models simulate the projected intensity of TCs and include the effect of poleward migration, this is only one of the contributing factors to TC's intensity change. In other words, poleward migration's effect is embedded, but not readily separable. To separate its effect, a reference case is required, such that the only difference between the two cases is the effect of poleward migration. However, it is challenging to set up that properly in climate model simulations without modifying other factors in such complex models.

This research thus proposes to use an alternative approach, the Potential Intensity[41–45] (PI) approach, to address the issue.

As will be shown, the advantage is that both the 'with' and 'without' poleward migration cases can be cleanly generated to separate and quantify poleward migration's effect on future TCs. PI is TC's intensity theoretical upper bound, given the thermal-dynamic environmental conditions. Though PI is not the actual intensity of TCs, it is the closest possible intensity estimate with strong theoretical underpinning[13,41]. It has also been suggested to

be used as a proxy for the actual intensity as well[13]. Thus the information provided is highly relevant, especially understanding how PI may change in the future is by itself important.

Our study region is the Western North Pacific Ocean (WNP), as it is among the global oceans where poleward migration is the most evident, in both present-day observation as well as in future projections[30–40]. The WNP is also the largest TC basin on earth: 60% of the world's most intense TCs (i.e., Category-5 TCs) are located in the WNP[46,47].

Before proceeding, we first perform a latitude analysis to re-examine the poleward migration over the WNP by the end of the 21st Century, to ensure that a robust poleward migration projection exists. Three TC track groups are examined. The first two groups are from the CMIP5 (Coupled Model Intercomparison Project 5) explicitly-simulated TCs, under the Representative Concentration Pathway (RCP) 4.5 and 8.5 emission pathways, as in Camargo 2013[5]. The third group of tracks is from synthetic TCs downscaled from the CMIP5 RCP 8.5 environmental fields, as in Emanuel 2015[8]. The first and the 2nd groups are named C-Track-4.5, and C-Track-8.5, respectively, while the 3rd group is named E-Track-8.5. Both C-Track-4.5 and C-Track-8.5 include 6 different climate models, while E-Track-8.5 includes 7 models. Although more models are included in Camargo 2013[5], some generate too few TCs and their climatology is too different from observations, therefore those models are excluded from analysis (Methods). All 7 models from Emanuel 2015[8] are considered here.

As we are interested in centennial trends, a 10-year low-pass running filter is applied to remove high-frequency (e.g. inter-annual) variability. Additional tests using 5-year and 20-year filters are also conducted. We arrange the data according to each consecutive 10-year period till century's end (2006–2015, 2007–2016… 2091–2100). We consider both a Multi-Model Ensemble (MME), as well as individual models in our analysis. Because our interest is on TC intensification, we define an

[1]Department of Atmospheric Sciences, National Taiwan University, Taipei, Taiwan. [2]Lamont-Doherty Earth Observatory, Columbia University, Palisades, NY, USA. [3]The Climate Service, Durham, NC, USA. [4]University of Wisconsin-Madison, Wisconsin-Madison, USA. ✉email: iilin@ntu.edu.tw

intensification track (IT) for each TC. IT is defined as the track points from the genesis location to the Lifetime Maximum Intensity (LMI) location. The IT points for C-Track-4.5/ C-Track-8.5 have 6-hourly intervals, while the E-Track-8.5 track points have 2-hourly intervals. All analyses in this research are based on the IT points (i.e., point-based analyses). From here onwards, 'track points' refer only to the IT points, and 'track locations' refer only to their locations.

All track locations are analysed to assess whether poleward migration is a general behaviour rather than just existing at the locations of the LMI[30]. Figure 1 illustrates the MME-average results for the latitude analysis. Statistically significant northward trends for all 3 track groups are found, and the migration rate is ~ 0.07°N, 0.13°N, and 0.16°N per decade for C-Track-4.5, C-Track 8.5, and E-Track 8.5, respectively. It can also be seen that the migration rate for the weaker emission group, i.e., C-Track-4.5, is smaller than the stronger emission group (C-Track 8.5), though still significant statistically. Individual-model results also show consistency, and the majority of the models have statistically significant northward trends (≥95%, 5/6, 4/6, 7/7 in Supplementary Figs. 1–3). These results confirm the necessity to explore the effect of poleward migration on future TCs' intensification.

Our idea is illustrated in Fig. 2. We construct and compare two types of future PI projection scenarios: one with and the other

without the poleward migration impact. The projection with (without) poleward migration is called TC_Move (TC_Stay). Both projections start at the present-day climate (defined as 2006–2015, Time 1 in Fig. 2). At Time 1, PIs are calculated at each of the present-day track locations, according to the corresponding Time-1 environmental input fields. Four inputs are required, namely sea surface temperature (SST), atmospheric temperature profile, atmospheric humidity profile, and sea level pressure[41]. At Time 2 (i.e., 2007–2016), environmental fields are updated, and the 2 scenarios split. For TC_Move, PIs are calculated at the new track locations of Time 2. For TC_Stay, however, PIs are still calculated at the same locations as in Time 1, since no spatial movement is involved. In other words, the track locations for TC_Stay are fixed throughout (Fig. 2_lower part), while the track locations for TC_Move are updated dynamically (Fig. 2_upper part).

Both types of PI projections are constructed for individual-model members as well as MME. There are different ways to generate the MME, we consider four approaches, called MME1-MME4, to ensure the robustness of our results and to explore their uncertainty. Because there are 3 track groups (C-Track-4.5, C-Track-8.5, E-Track-8.5), and each has 4 MMEs, we have 12 MMEs for comprehensive assessment. As will be shown, the results are consistent across the four approaches. For simplicity, the
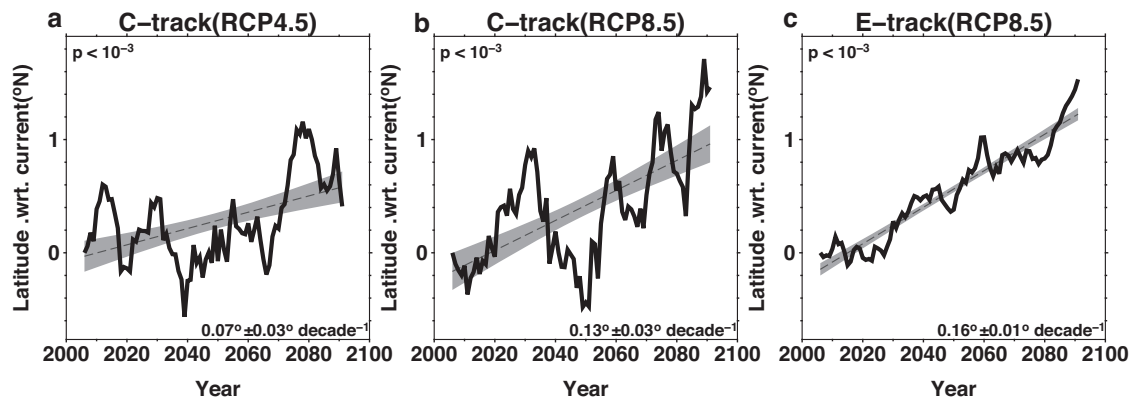

Fig. 1   Latitude time series. MME-averaged latitude time series of the 3 TC track groups, with trends and *p*-values. 95% confidence trend bounds are shaded.
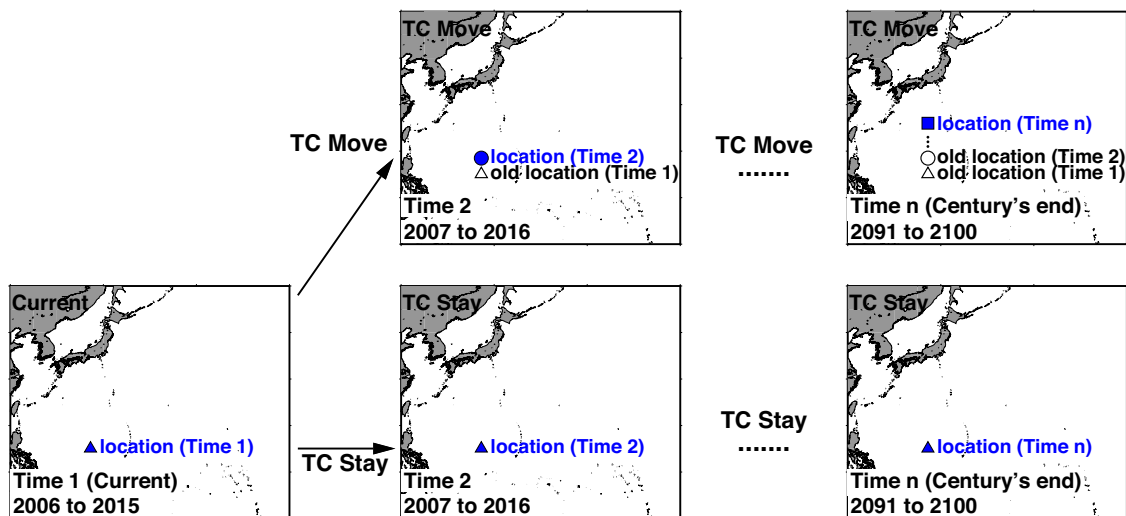

Fig. 2   Schematic diagram comparing the 2 PI projection scenarios. TC_Stay (i.e., no poleward migration) vs. TC_Move (poleward migration included) projections. For simplicity, only one TC track location (in blue) is shown to represent the TC locations at any given time.

discussion will be primarily based on MME1 with the results from the other MMEs shown in Supplementary Figs. 4, 5. Also as mentioned, the main results are based on a 10-year low-pass filter, 5-year and 20-year filters are also tested. The results are similar, as in Supplementary Figs. 6–9.

RESULTS

Proportion of Category-5 PI trends

For each consecutive 10-year time period, we have a group of PI samples, i.e., one corresponding PI value for each TC track location. We define "Proportion of Category-5 PI" as the percentage of Category-5 PI samples relative to the total PI samples. This represents the chance of intensification to the highest intensity category 5, among all the samples. Figure 3a–c depict the results, based on MME1. Without poleward migration (i.e., the TC_Stay projection), robust increasing trends for all three RCP/track groups are found, as climate warms (red curves). When poleward migration is included (the TC_Move projection), the increasing trends are still evident and statistically significant, though weaker (black curves). For instance in Fig. 3c (E-Track-8.5), the trend slope is $2.92 \pm 0.13\%$ decade^{-1} for TC_Stay and $1.94 \pm 0.11\%$ decade^{-1} for TC_Move. The difference between these two slopes is 0.98, equivalent to ~ 34% (0.98/2.92) decrease compare to TC_Stay.

In Table 1, the overall decrease (weakening) of the trend slope (including MME1 to MME4) for C-Track-4.5, C-Track-8.5, and E-Track-8.5 is −4 to −37%, −30 to −87%, and −30 to −47%. These results suggest that poleward migration does have an appreciable and considerable negative impact on future PIs, by weakening the increasing trends though not reversing their sign. The mean weakening in trend slope for RCP 8.5 (i.e., including the 8 MMEs in C-Track-8.5 and E-Track-8.5) is 42% and for RCP 4.5 is 22% (Table 1). In other words, the increase in the proportion of

Category-5 PI under RCP 8.5 (RCP 4.5) may only be about 58% (78%) of what is projected when the poleward migration of TCs is not taken into account.

Because the difference between TC_Move and TC_Stay is poleward migration's impact, we depict this difference in the lower panels of Fig. 3. It can be seen that the stronger the emission, the stronger the negative effect of poleward migration (Fig. 3d, e, i.e. comparing RCP 4.5 and 8.5 for C-Track). Furthermore, the poleward migration's negative impact can be seen in both RCP 4.5 and RCP 8.5, albeit with different magnitude, echoing the latitude analysis that the amount of poleward migration is larger in RCP 8.5 than in RCP 4.5 (Fig. 1a, b).

Average PI trends

We now consider the average PI, defined as the average from all PI samples in each consecutive 10-year time period. Similar to the results above, the average PI trends are smaller, when the poleward migration is included, though their signs are still positive (Fig. 4a–c). Consistently, the stronger the emission pathway, the stronger the negative effect of the poleward migration on average PI (Fig. 4d, e). The overall trend weakening for C-Track-4.5, C-Track-8.5, and E-Track-8.5 is −7 to −44%, −67 to −97%, and −56 to −65% (Table 2). The mean weakening for RCP 8.5 (i.e., including the 8 MMEs in C-Track-8.5 and E-Track-8.5) is 68% and for RCP 4.5 is 30% (Table 2). In other words, the increase in the average PI under RCP 8.5 (RCP 4.5) may only be about 32% (70%) of the PI projections which do not consider the poleward migration of TCs.

It should be noted that though the average PI increases little in the TC_Move projection (e.g., black curve in Fig. 4c), it does not mean that the increase in the high PIs is as little. As in the black curve of Fig. 3c, the proportion of Category-5 PI still increases considerably. The reason for the less increase in the averaged PI w.r.t. current is because PI distribution change is involved, and the
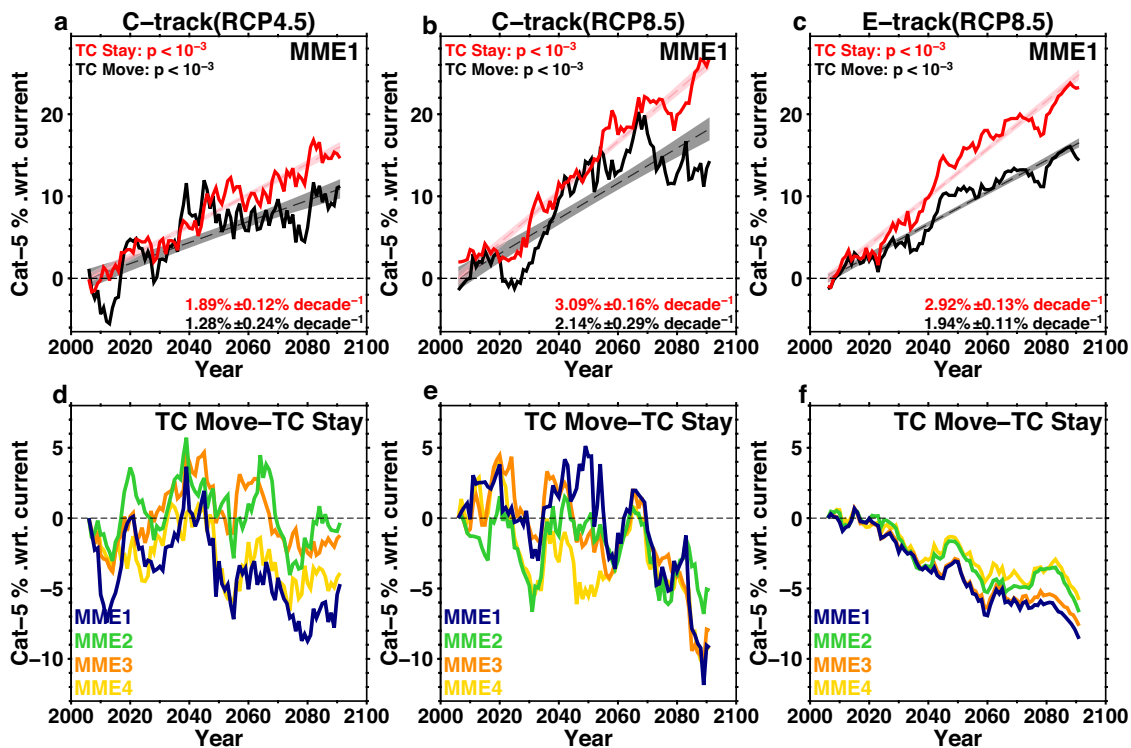

Fig. 3 Time series of the portion of Category-5 PI (i.e. Category-5 PI count over total PI count). Top (**a**, **b**, **c**): Proportion of Category-5 PI time series of the 3 track groups, with trends and p-values, based on MME1. 95% confidence trend bounds are shaded. The regression lines are aligned at the zero point for trend comparison. Bottom (**d**, **e**, **f**): The difference between TC_Move and TC_Stay, i.e., poleward migration's negative effect, for the 3 track groups. All 4 MMEs are depicted.

Table 1. Trend results of the Proportion of Category-5 PI.

	Proportion of Category-5 PI (%)											
	C-Track-4.5				C-Track-8.5				E-Track-8.5			
	MME1	MME2	MME3	MME4	MME1	MME2	MME3	MME4	MME1	MME2	MME3	MME4
TC Stay trend slope, p	$1.89 \pm 0.12\%$ decade^{-1}, $p < 10^{-3}$	$0.91 \pm 0.09\%$ decade^{-1}, $p < 10^{-3}$	$2.14 \pm 0.14\%$ decade^{-1}, $p < 10^{-3}$	$1.08 \pm 0.17\%$ decade^{-1}, $p < 10^{-3}$	$3.09 \pm 0.16\%$ decade^{-1}, $p < 10^{-3}$	$0.91 \pm 0.11\%$ decade^{-1}, $p < 10^{-3}$	$3.22 \pm 0.17\%$ decade^{-1}, $p < 10^{-3}$	$1.04 \pm 0.16\%$ decade^{-1}, $p < 10^{-3}$	$2.92 \pm 0.13\%$ decade^{-1}, $p < 10^{-3}$	$1.52 \pm 0.08\%$ decade^{-1}, $p < 10^{-3}$	$2.98 \pm 0.13\%$ decade^{-1}, $p < 10^{-3}$	$1.57 \pm 0.08\%$ decade^{-1}, $p < 10^{-3}$
TC Move trend slope, p	$1.28 \pm 0.24\%$ decade^{-1}, $p < 10^{-3}$	$0.77 \pm 0.21\%$ decade^{-1}, $p < 10^{-3}$	$2.06 \pm 0.22\%$ decade^{-1}, $p < 10^{-3}$	$0.68 \pm 0.20\%$ decade^{-1}, $p < 10^{-3}$	$2.14 \pm 0.29\%$ decade^{-1}, $p < 10^{-3}$	$0.55 \pm 0.21\%$ decade^{-1}, $p < 10^{-3}$	$2.24 \pm 0.24\%$ decade^{-1}, $p < 10^{-3}$	$0.14 \pm 0.25\%$ decade^{-1}, 0.266	$1.94 \pm 0.11\%$ decade^{-1}, $p < 10^{-3}$	$0.81 \pm 0.08\%$ decade^{-1}, $p < 10^{-3}$	$2.09 \pm 0.11\%$ decade^{-1}, $p < 10^{-3}$	$0.96 \pm 0.08\%$ decade^{-1}, $p < 10^{-3}$
Weakening impact	$(1.28–1.89)$/$1.89 = −32\%$	$(0.77–0.91)$/$0.91 = −15\%$	$(2.06–2.14)$/$2.14 = −4\%$	$(0.68–1.08)$/$1.08 = −37\%$	$(2.14–3.09)$/$3.09 = −31\%$	$(0.55–0.91)$/$0.91 = −40\%$	$(2.24–3.22)$/$3.22 = −30\%$	$(0.14–1.04)$/$1.04 = −87\%$	$(1.94–2.92)$/$2.92 = −34\%$	$(0.81–1.52)$/$1.52 = −47\%$	$(2.09–2.98)$/$2.98 = −30\%$	$(0.96–1.57)$/$1.57 = −39\%$
Overall weakening impact	$−4$ to $−37\%$ Mean Value ($−22\%$)				$−30$ to $−87\%$ Mean Value ($−47\%$)				$−30$ to $−47\%$ Mean Value ($−38\%$)			

- For RCP 4.5, the weakening impact mean value is −22% (based on the 4 MMEs from C-Track-4.5).
- For RCP 8.5, the weakening impact mean value is −42% (based on 8 MMEs, i.e., 4 MMEs each, from C-Track-8.5 and E-Track-8.5).
- Poleward migration's weakening impact is defined as (trend slope of TC Move - trend slope of TC Stay)/trend slope of TC Stay, because TC Stay is the reference scenario.

increase in the high and low PI samples compensate each other (see next section and Fig. 5d, f). Another point to note is that recent report suggested that the observed emission so far appears to match more closely with the RCP 8.5 pathway[48]. Kossin's (2015)[45] study in the present climate also suggested a considerable modulation by poleward migration of the observed average PI.

Lastly, it can be seen in Fig. 4 that multi-decadal variability is also visible. As in Fig. 1, multi-decadal variability plays a part in modulating the TC track as warming progresses. These suggest that for the western North Pacific TCs, besides the global warming signal, multi-decadal signal is likely to continue to play a considerable role in jointly modulating TC variability in the future, including track and PI.

The offsetting effect of poleward migration

Figure 5a presents the TC-Season averaged PI map in the current climate, with present-day TC locations overlaid as enclosed by the black contour (enclosed 95% of TC IT points). As the climate warms, PI increases (Fig. 5b). If the TC location shifts are not included, there is a net increase in PI, because the PI values enclosed by the black contour in Fig. 5b increase, as compared to the PI values enclosed by the same black contour in Fig. 5a. This is the well-known increase in PI due to anthropogenic climate change (e.g. Sobel et al. 2016)[13]. However, if poleward migration is considered, future TCs will concurrently migrate northward into a region of lower PI values (enclosed by the white contour in Fig. 5c). Therefore, the PI values enclosed by the white contour in Fig. 5c have a higher contribution from the lower PI values to the north, when comparing with the PI values enclosed by the black contour in Fig. 5b. In other words, the poleward migration has a negative influence on PI, offsetting global warming's positive influence, and PI projection TC_Move is the result of these 2 competing factors (Fig. 5c). Comparing the two PI projections, the TC_Stay projection only includes global warming's influence in increasing future PI values (Fig. 5b). In contrast, TC_Move PI projection (Fig. 5c), both the global warming's positive influence and poleward migration's negative influence are at work to determine future PIs. This can also be seen in the PI distribution where increases in both the high and low-ends of the spectrum w.r.t. current are found (Fig. 5d, f).

DISCUSSION

This research quantifies the impact of poleward migration on future WNP TC's intensification via two contrasting PI projections. Without poleward migration, at the end of the 21st century, the estimated increase in the proportion of Category-5 PI (average PI) w.r.t. current is ~ 18.3% (2.7 m s^{-1}) under RCP 8.5 (Supplementary Table 1). With poleward migration, the estimated increase in the proportion of Category-5 PI (average PI) at century's end w.r.t. current would only be ~11.6% (0.8 m s^{-1}). For RCP 4.5, without and with poleward migration, the estimated increase in the proportion of Category-5 PI at century's end w.r.t. current is 12.8% vs. 10.2%, and 2.3 m s^{-1} vs. 1.6 m s^{-1} for average PI (Supplementary Table 2).

Outside the PI framework analysed above, there are other environmental factors which may also change with poleward migration and could affect future TCs, such as ocean subsurface stratification[9] and vertical wind shear[49]. Although these effects are not main scope of this study, we conducted some preliminary assessment. Environmental fields of two E-Track-8.5 models, SP-CCSM4 and HADGEMS2-ES, are examined. The results from the 2 models are consistent (Supplementary Note 1, Supplementary Fig. 10–12). A brief summary based on SP-CCSM4 is given below.

We found that there is an increase in ocean subsurface stratification as TCs move northwards (Supplementary Note 1). Using ocean profiles averaged along the IT points during the TC-
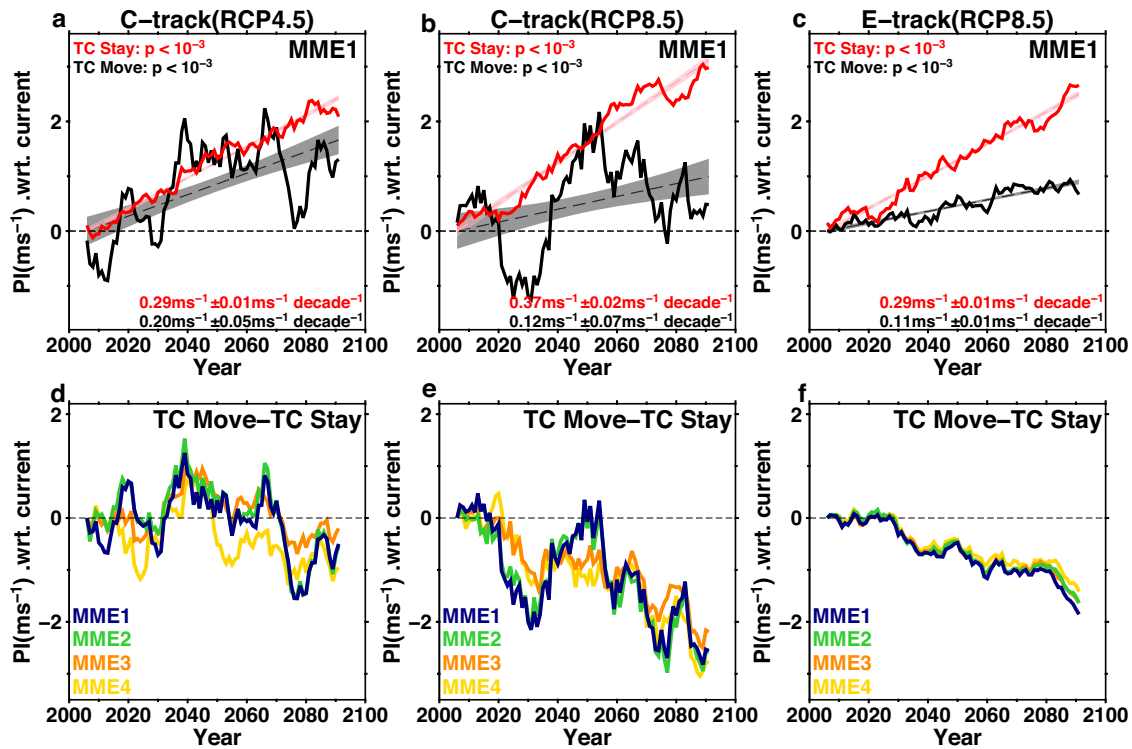
Fig. 4 Time series of Averaged PI. Top (**a**, **b**, **c**): Averaged PI time series of the 3 track groups, with trends and p-values, based on MME1. 95% confidence trend bounds are shaded. The regression lines are aligned at the zero point for trend comparison. Bottom (**d**, **e**, **f**): The difference between TC_Move and TC_Stay, i.e., poleward migration's negative effect, for the 3 track groups. All 4 MMEs are depicted.

Season (June-November) in with and without poleward migration situation, we employed the 3D Price-Weller-Pinkel (3DPWP) ocean model[50] to estimate the TC-induced ocean cooling effect[46,50,51]. The cooling effect from both entrainment mixing and upwelling are included in the 3DPWP. 3DPWP is run at TC translation speed of 5 m s^{-1}. After obtaining the cooling effect, we used the Ocean Coupling Potential Intensity (OCPI)[52,53], i.e., a revised PI index, which incorporates the subsurface contribution to PI. The results show that 'with' and 'without' subsurface contribution, poleward migration's negative effect (i.e., the difference between TC_Stay and TC_Move) on average PI is −0.95 m s^{-1} vs. −0.86 m s^{-1}. This suggests that subsurface factor does contribute to the negative effect, though may not be too large (−0.09 m s^{-1}, Supplementary Note 1). It also suggests that the effect of poleward migration estimated in the PI analysis should be smaller than in the actual intensity, because there are additional negative factors such as ocean subsurface contribution to add-on to the negative effect. Nevertheless, PI should still have captured the main effect, because the 'add-on' effect from ocean subsurface does not appear to be overly large. Further investigation using more models is needed.

In the case of vertical wind shear, it can be seen in Supplementary Fig. 11 that even when poleward migration (grey contour) is considered, most TC locations are still distant from the region of very high shear at 30–50°N. With and without poleward migration, the average shear values are 9.8 and 9.9 m s^{-1}, respectively. Again, further investigation using more models is needed.

Nature is an extremely complex system. The occurrence of poleward migration can partially offset global warming's positive impact on future WNP TCs, the stronger the global warming, the larger the poleward shift, the stronger the negative impact from poleward migration to offset corresponds. These results suggest that at least over the largest TC basin on Earth, future TCs may not intensify without constraint as warming progresses, because a concurrent negative process (poleward migration) also projected to exist to jointly control future WNP TC's intensification. When simulating WNP TC intensity in the future, it is important to consider this effect from poleward migration, to avoid over-estimation of TC intensity increase.

METHODS

Study area
120–180°E, 0–90°N.

Study period
2006–2100.

TC season
June-November (6 months). All analyses in this research are TC-Season based.

Current and future conditions
Current: 2006–2015, Future: 2091–2100. The reason to use the first and the last 10 years to represent current and future is because CMIP5's projection period is from 2006 to 2100 (95 years). If taking the first and the last 10 years, there are still 76 year's gap between current and future. If we take the first and the last 20 years (i.e. 2006–2025 and 2081–2100), the gap between current and future will be too short (i.e., only 56 years). Nevertheless, as in Supplementary Fig. 6 and Supplementary Fig. 7, we also test the 20-year results, and the results are consistent.

Saffir–Simpson Tropical Cyclone Scale
Saffir–Simpson tropical cyclone scale based on the 1-min maximum sustained winds: Category 1: 64–82 kts (33–42 m s^{-1}), Category 2: 83–95 kts (43- <49 m s^{-1}), Category 3: 96–112 kts (49-

Table 2. Trend results of averaged PI.

	C-Track-4.5				C-Track-8.5				E-Track-8.5			
Avg. PI (m s⁻¹)	MME1	MME2	MME3	MME4	MME1	MME2	MME3	MME4	MME1	MME2	MME3	MME4
TC stay trend slope, p	0.29 ± 0.01 decade⁻¹, $p < 10^{-3}$	0.27 ± 0.01 decade⁻¹, $p < 10^{-3}$	0.27 ± 0.01 decade⁻¹, $p < 10^{-3}$	0.26 ± 0.01 decade⁻¹, $p < 10^{-3}$	0.37 ± 0.02 decade⁻¹, $p < 10^{-3}$	0.36 ± 0.02 decade⁻¹, $p < 10^{-3}$	0.36 ± 0.02 decade⁻¹, $p < 10^{-3}$	0.32 ± 0.02 decade⁻¹, $p < 10^{-3}$	0.29 ± 0.01 decade⁻¹, $p < 10^{-3}$	0.26 ± 0.01 decade⁻¹, $p < 10^{-3}$	0.30 ± 0.01 decade⁻¹, $p < 10^{-3}$	0.27 ± 0.01 decade⁻¹, $p < 10^{-3}$
TC move trend slope, p	0.20 ± 0.05 decade⁻¹, $p < 10^{-3}$	0.15 ± 0.06 decade⁻¹, $p < 10^{-3}$	0.25 ± 0.04 decade⁻¹, $p < 10^{-3}$	0.16 ± 0.04 decade⁻¹, $p < 10^{-3}$	0.12 ± 0.07 decade⁻¹, $p < 10^{-3}$	0.10 ± 0.06 decade⁻¹, 0.001	0.12 ± 0.03 decade⁻¹, $p < 10^{-3}$	0.01 ± 0.04 decade⁻¹, 0.651	0.11 ± 0.01 decade⁻¹, $p < 10^{-3}$	0.09 ± 0.01 decade⁻¹, $p < 10^{-3}$	0.13 ± 0.01 decade⁻¹, $p < 10^{-3}$	0.12 ± 0.01 decade⁻¹, $p < 10^{-3}$
Weakening impact	(0.20–0.29) /0.29 = −31%	(0.15–0.27) /0.27 = −44%	(0.25–0.27) /0.27 = −7%	(0.16–0.26) /0.26 = −38%	(0.12–0.37) /0.37 = −68%	(0.10–0.36) /0.36 = −72%	(0.12–0.36) /0.36 = −67%	(0.01–0.32) /0.32 = −97%	(0.11–0.29) /0.29 = −62%	(0.09–0.26) /0.26 = −65%	(0.13–0.30) /0.30 = −57%	(0.12–0.27) /0.27 = −56%
Overall weakening impact	−7 to −44% Mean Value (−30%)				−67 to −97% Mean Value (−76%)				−56 to −65% Mean Value (−60%)			

Poleward migration's weakening impact is defined as: (trend slope of TC Move - trend slope of TC Stay)/trend slope of TC Stay, because TC Stay is the reference scenario.
• For RCP 4.5, the weakening impact mean value is −30% (based on the 4 MMEs from C-Track-4.5).
• For RCP 8.5, the weakening impact mean value is −68% (based on 8 MMEs, i.e., 4 MMEs each, from C-Track-8.5 and E-Track-8.5).

<58 m s⁻¹), Category 4: 113–136 kts (58- <71 m s⁻¹), and Category 5: $\geqq$ 137 kts (71 m s⁻¹). Related classifications for Tropical Depression (TD): $\leqq$ 33 kts (17 m s⁻¹), Tropical Storm (TS): 34–63 kts (18–32 m s⁻¹).

TC track groups and CMIP-5 model members

As in text, three groups of projected TC tracks are used: C-Tracks-4.5, C-Tracks-8.5 from Camargo 2013;[5] and E-Tracks-8.5 from Emanuel 2015[8]. As in Camargo 2013[5], some CMIP5 models generate too few TCs and their climatology is too different from observations. Therefore, for C-Tracks-4.5 and C-Tracks-8.5, models with fewer than 2 TCs per year in the current climate (2006–2015) or with more than 15 years of no TCs in the entire projection period (2006–2100) are excluded from our analysis. The final 6 models for C-Track-4.5 are: CanESM2, CSIRO Mk3.6.0, GFDL-CM3, GFDL-ESM2M, HadGEM2-ES, MRI-CGCM3; for C-Track-8.5 are: CSIRO Mk3.6.0, GFDL-CM3, GFDL-ESM2M, HadGEM2-ES, IPSL-CM5A-LR, MRI-CGCM3. For E-Track-8.5, by construction this low bias is not present and all 7 models in Emanuel 2015[8] are used. They are: GFDL-CM3, HadGEM2-ES, IPSL-CM5A-LR, MIROC5, MPI-ESM-MR, MRI-CGCM3, SP-CCSM4.

For C-Track-4.5 and C-Track-8.5, there are 2 model members from the same institution, i.e., GFDL (Geophysical Fluid Dynamic Laboratory). Therefore, concerning the issue of possible over-representation from a single institution[40,54–56] (models not being fully independent), we first combine the 2 GFDL models (GFDL-CM3 and GFDL-ESM2M) as one entity, called GFDL-MME (Multi-Model Ensemble), to represent GFDL.

Latitude and longitude analyses

For each consecutive 10-year period (2006–2015, 2007–2016… 2091–2100), there is a group of TC locations, and a latitude average is calculated. After obtaining individual-model latitude time series, the MME average is obtained via averaging the individual time series. Similar analysis was conducted for the longitude[57] time series (Supplementary Figs. 14, 15).

PI projections and multi-model ensembles (MMEs)

As in the text, 2 contrasting PI projections, i.e. TC_Stay (no poleward migration) and TC_Move (poleward migration included) are constructed. For convenience, we first generate a series of TC-season, 10-year average PI maps (2006–2015, 2007–2016,… 2091–2100) for each model (called 'model PI maps'). For each track group, we also generate a series of MME PI maps (called 'MME PI maps') via averaging the respective set of the model PI maps. The methodology is similar to Sobel et al. 2016[13]. Monthly PI map is first built using monthly input fields from CMIP5 environmental atmospheric temperature/humidity profiles, sea level pressure, and SST. The grid size is 1 by 1. The original PI program is from K. Emanuel at MIT (ftp://texmex.mit.edu/pub/emanuel/TCMAX/pcmin_2013.f)[41], and is run at each grid to build the monthly map.

After constructing the PI maps, we extract PI values at TC track locations from the PI maps. For TC_Stay, the same present-day (2006–2015) track locations are used throughout updated PI maps (Supplementary Fig. 16). For TC_Move, PI values are extracted from updated PI maps at updated TC locations (Supplementary Fig. 17).

Because there can be different approaches to generate the MME, for each track group, four approaches are applied. We consider two aspects, pre-rescaling of TC track points and sequence in PI map extraction. As each aspect has 2 options, there are 4 MMEs (Supplementary Table 3). The 2 options for pre-rescaling of track points are: 'Yes' and 'No'. The option for 'No' (i.e., no pre-rescaling) is the direct composition using the original TC track points from individual-model members. However, because
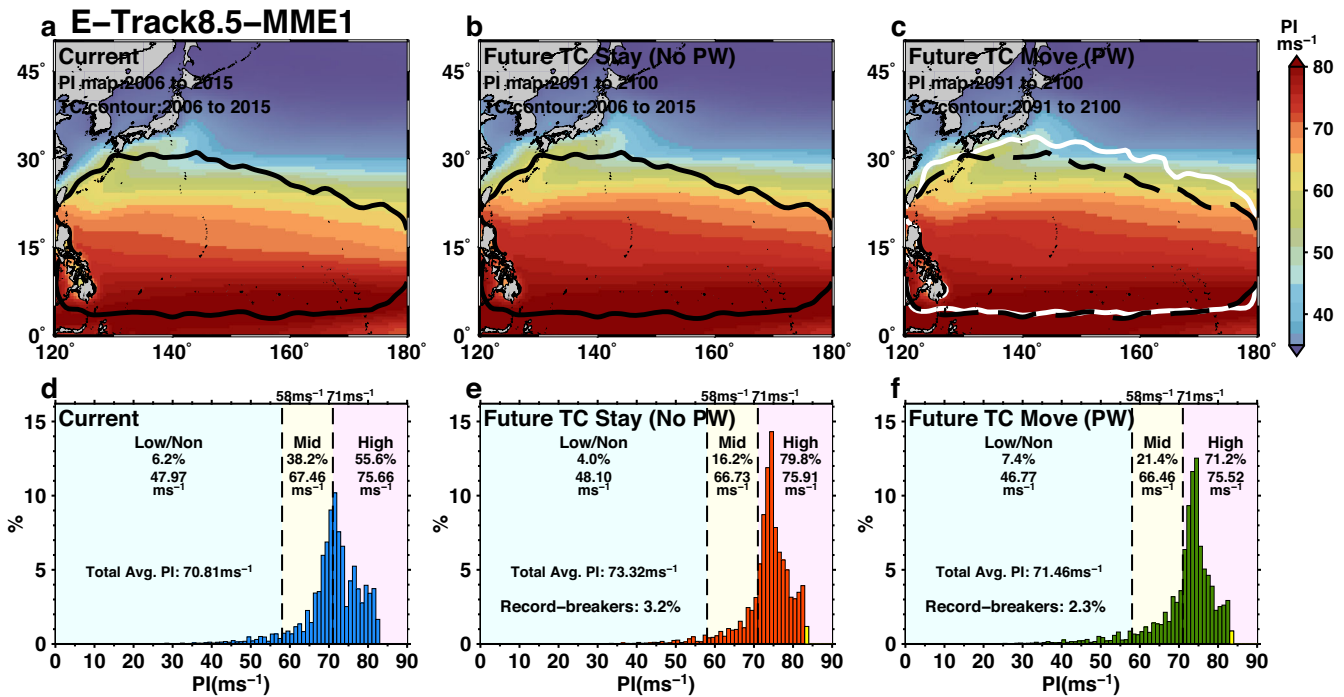
Fig. 5 PI distribution and poleward migration. Comparison between current (**a**) and the 2 future PI scenarios (**b**, **c**), based on E-Track-8.5 MME1. The background map in colour is the TC-Season averaged PI map. TC location contour, based on intensification-track points, is overlaid. These points are first interpolated to 2 by 2 grid before contouring, 95% of points are enclosed. **a** Current: present-day PI map with present-day TC location contour overlaid. **b** Future TC_Stay: future PI map with present-day TC location contour (in black) overlaid. This contour is the same as in (**a**), because there is no TC movement involved. **c** Future TC_Move: future PI map with future TC location contour (in white) overlaid. The contour in (**b**) is also shown in dashed black, for comparison. **d**–**f** PI probability distribution histogram for Current (**d**), future TC_Stay (**e**), and future TC_Move (**f**). Additional discussions see Supplementary Note 2.

the original point counts among individual models can be vastly different (see rows 2/3 in Tables a/b of Supplementary Tables 4–6), this type of direct composition can have a bias towards model members with more track points, while overwhelming the contributions from members with fewer track points. Thus, we also consider the 'Yes' option, i.e. pre-rescaling the track points to equalize the contributions from individual-model members to MME (i.e., equal-weighting). Technical details see section below.

As for the sequence in PI map extraction, there are 2 options: Option 1 and Option 2. Option 1 extracts PI values from the MME PI maps, based on the MME composited track locations (e.g., see Supplementary Fig. 13). Option 2 first extracts PI values from individual-model PI maps using individual-model track locations, then combines together to form MME.

Pre-rescaling of TC Track Points

Pre-rescaling of track points is summarized in Supplementary Tables 4–6. Using C-Track-8.5 as an example, we explain the concept. As in Supplementary Table 5, the original track point counts among the individual-model members are vastly different. For example, the CSIRO model alone contributes ~37.1% to MME, 7 times the contribution from IPSL (5.7%) (row 3 in Supplementary Table 5b). Though direct composition using original track points (i.e. no pre-rescaling) is intuitive, it is a non-equal-weighting approach, and there is a bias towards big models such as CSIRO. To establish an equal-weighting approach, TC track points from individual models are pre-rescaled to equal base, before compositing.

We first choose a count reference close to the mean count among the model members. For example, the count reference for C-Track-8.5 is 2600, as the original counts are between 960 to 4523 (row 2 of Supplementary Table 5a). The rescaling is thus to scale the individual model counts towards 2600 (rows 5 in

Supplementary Table 5a). Using the HadGEMS2-ES model as an example, our approach is illustrated. We first place the TC IT points over a map of grid size 1 by 1 (Supplementary Fig. 18). Because the original TC count is 1582, the rescaling factor is 1.643 (2600/1582). Therefore for each grid, we multiply the count by the rescaling factor. As in Supplementary Fig. 18b, the spatial features and patterns are still preserved after rescaling, because it is only a linear scaling. After rescaling, the count is 2681, i.e. ~2600. The reason why it can not be exactly 2600 is because at each grid, the count has to be an integer after rescaling, thus there is some minor difference.

After rescaling for current (2006–2015, Supplementary Fig. 18a, b), rescaling is also done for all subsequent 10-year tracks (2007–2016,…2091–2100). The result for 2091–2100 is shown in Supplementary Fig. 18c, d. This approach is applied to all individual models. After rescaling, all 5 members (CSIRO Mk3.6.0, GFDL-MME, HadGEM2-ES, IPSL-CM5A-LR, MRI-CGCM3) have ~2600 points, corresponding to ~20% equal contribution to the C-Track-8.5 MME (row 6 in Supplementary Table 5a, b). This approach thus enables feature preservation and yet able to bring models with large initial point count difference to equal basis. In addition, because current and future track points are both rescaled to ~2600, it has the additional benefit of ensuring that the change in track points between current and future is due to change in location alone, and not from TC frequency change between future and current[33].

TC-induced ocean cooling effect

The TC-induced ocean cooling effect is estimated using the 3DPWP ocean model[50]. The wind forcing is based on the intensification-track averaged TC-Season climatological (1980–2019) wind speed from the US Joint Typhoon Warning Center. TC translation speed used is 5 m s^{-1}.

Vertical wind shear

Vertical wind shear (VWS) is calculated based on the 850 and 200 hPa wind difference over the WNP domain, at each 1 by 1 grid.

DATA AVAILABILITY

CODE AVAILABILITY

REFERENCES

1. Knutson, T. R. & Tuleya, R. E. Impact of CO_2-induced warming on simulated hurricane intensity and precipitation: Sensitivity to the choice of climate model and convective parameterization. *J. Clim.* **17**, 3477–3495 (2004).
2. Emanuel, K. Increasing destructiveness of tropical cyclones over the past 30 years. *Nature* **436**, 686–688 (2005).
3. Knutson, T. R. et al. Tropical cyclones and climate change. *Nat. Geosci.* **3**, 157–163 (2010).
4. Murakami, H. et al. Future changes in tropical cyclone activity projected by the new high-resolution MRI-AGCM. *J. Clim.* **25**, 3237–3260 (2012).
5. Camargo, S. J. Global and regional aspects of tropical cyclone activity in the CMIP5 models. *J. Clim.* **26**, 9880–9902 (2013).
6. Emanuel, K. A. Downscaling CMIP5 climate models shows increased tropical cyclone activity over the 21st century. *Proc. Natl Acad. Sci. USA* **110**, 12219–12224 (2013).
7. Lin, I. I., Pun, I. F. & Lien, C. C. 'Category-6' supertyphoon Haiyan in global warming hiatus: contribution from subsurface ocean warming. *Geophys. Res. Lett.* **41**, 8547–8553 (2014).
8. Emanuel, K. A. Effect of upper-ocean evolution on projected trends in tropical cyclone activity. *J. Clim.* **28**, 8165–8170 (2015).
9. Huang, P., Lin, I. I., Chou, C. & Huang, R.-H. Change in ocean subsurface environment to suppress tropical cyclone intensification under global warming. *Nat. Commun.* **6**, 7188 (2015).
10. Knutson, T. R. et al. Global projections of intense tropical cyclone activity for the late twenty-first century from dynamical downscaling of CMIP5/RCP4.5 scenarios. *J. Clim.* **28**, 7203–7224 (2015).
11. Lin, I. I. & Chan, J. C. L. Recent decrease in typhoon destructive potential and global warming implications. *Nat. Commun.* **6**, 7182 (2015).
12. Mei, W. & Xie, S.-P. Intensification of landfalling typhoons over the northwest Pacific since the last 1970s. *Nat. Geosci.* **9**, 753–757 (2016).
13. Sobel, A. H. et al. Human influence on tropical cyclone intensity. *Science* **353**, 242 (2016).
14. Tuleya, R. E. et al. Impact of upper-tropospheric temperature anomalies and vertical wind shear on tropical cyclone evolution using an idealized version of the operational GFDL hurricane model. *J. Atmos. Sci.* **73**, 3803–3820 (2016).
15. Walsh, K. J. E. et al. Tropical cyclones and climate change. *WIRES Clim. Change* **7**, 65–89 (2016).
16. Korty, R. L., Emanuel, K. A., Huber, M. & Zamora, R. A. Tropical cyclones downscaled from simulations with very high carbon dioxide levels. *J. Clim.* **30**, 649–667 (2017).
17. Yoshida, K., Sugi, M., Mizuta, R., Murakami, H. & Ishii, M. Future changes in tropical cyclone activity in high-resolution large-ensemble simulations. *Geophys. Res. Lett.* **44**, 9910–9917 (2017).
18. Bhatia, K., Vecchi, G., Murakami, H., Underwood, S. & Kossin, J. Projected response of tropical cyclone intensity and intensification in a global climate model. *J. Clim.* **31**, 8281–8303 (2018).
19. Patricola, C. M. & Wehner, M. F. Anthropogenic influences on major tropical cyclone events. *Nature* **563**, 339–346 (2018).
20. Knutson, T. et al. Tropical cyclones and climate change assessment: Part II. Projected response to anthropogenic warming. *Bull. Am. Meteor. Soc.* **101**, E303–E322 (2020).
21. Vecchi, G. et al. Tropical cyclone sensitivities to CO_2 doubling: roles of atmospheric resolution, synoptic variability and background climate changes. *Clim. Dyn.* **53**, 5999–6033 (2019).
22. Kossin, J. P., Knapp, K. R., Olander, T. L. & Velden, C. S. Global increase in major tropical cyclone exceedance probability over the past four decades. *Proc. Natl Acad. Sci. USA* **117**, 11975–11980 (2020).
23. Lee, C. Y., Camargo, S. J., Sobel, A. H. & Tippett, M. K. Statistical-dynamical downscaling projections of tropical cyclone activity in a warming climate: two diverging genesis scenarios. *J. Clim.* **33**, 4815–4834 (2020).
24. Lin, I. I. et al. *El Niño Southern Oscillation in a Changing Climate* Ch. 17 (John Wiley & Sons, Inc., 2020).
25. Murakami, H. et al. Detected climate change in global distribution of tropical cyclones. *Proc. Natl Acad. Sci. USA* **117**, 10706–10714 (2020).
26. Cha, E. J. et al. Third assessment on impacts of climate change on tropical cyclones in the typhoon committee region—Part II: future projections. *Trop. Cyclone Res. Rev.* **9**, 75–86 (2020).
27. Wang, S., Rashid, T., Thorp, H. & Toumi, R. A shortening of the life-cycle of major tropical cyclones. *Geophys. Res. Lett.* **47**, e2020GL088589 (2020).
28. Emanuel, K. A. Response of global tropical cyclone activity to increasing CO_2: Results from downscaling CMIP6 models. *J. Clim.* **34**, 57–70 (2021).
29. Roberts, M. J. et al. Projected future changes in tropical cyclones using the CMIP6 HighResMIP multimodel ensemble. *Geophys. Res. Lett.* **47**, e2020GL088662 (2020).
30. Kossin, J. P., Emanuel, K. A. & Vecchi, G. A. The poleward migration of the location of tropical cyclone maximum intensity. *Nature* **509**, 349 (2014).
31. Colbert, A. J., Soden, B. J. & Kirtman, B. P. The impact of natural and anthropogenic climate change on western north Pacific tropical cyclone tracks. *J. Clim.* **28**, 1806–1823 (2015).
32. Moon, I. J., Kim, S. H., Klotzbach, P. & Chan, J. C. L. Roles of interbasin frequency changes in the poleward shift of the maximum intensity location of tropical cyclones. *Environ. Res. Lett.* **10**, 104004 (2015).
33. Kossin, J. P., Emanuel, K. A. & Camargo, S. J. Past and projected changes in western north Pacific tropical cyclone exposure. *J. Clim.* **29**, 5725–5739 (2016).
34. Studholme, J. et al. Poleward expansion of tropical cyclone latitudes in warming climates. *Nat. Geosci.* **15**, 14–28 (2022).
35. Nakamura, J. et al. Western north Pacific tropical cyclone model tracks in present and future climates. *J. Geophys. Res—Atmos.* **122**, 9721–9744 (2017).
36. Altman, J. et al. Poleward migration of the destructive effects of tropical cyclones during the 20th century. *Proc. Natl Acad. Sci. USA* **115**, 11543–11548 (2018).
37. Sharmila, S. & Walsh, K. J. E. Recent poleward shift of tropical cyclone formation linked to Hadley cell expansion. *Nat. Clim. Change* **8**, 730–736 (2018).
38. Song, J. & Klotzbach, P. J. What has controlled the poleward migration of annual averaged location of tropical cyclone lifetime maximum intensity over the western north Pacific since 1961? *Geophys. Res. Lett.* **45**, 1148–1156 (2018).
39. Wang, S. & Toumi, R. Recent migration of tropical cyclones toward coasts. *Science* **371**, 514–517 (2021).
40. Bell, S. S. et al. Western north Pacific tropical cyclone tracks in CMIP5 models: statistical assessment using a model-independent detection and tracking scheme. *J. Clim.* **32**, 7191–7208 (2019).
41. Bister, M. & Emanuel, K. Low frequency variability of tropical cyclone potential intensity 1. Interannual to interdecadal variability. *J. Geophys. Res.* **107**, 4801 (2002).
42. Vecchi, G. A. & Soden, B. J. Effect of remote sea surface temperature change on tropical cyclone potential intensity. *Nature* **450**, 1066–1070 (2007).
43. Kossin, J. P. & Camargo, S. J. Hurricane track variability and secular potential intensity trends. *Clim. Change* **97**, 329 (2009).
44. Yu, J., Wang, Y. & Hamilton, K. Response of tropical cyclone potential intensity to a global warming scenario in the IPCC AR4 CGCMs. *J. Clim.* **23**, 1354–1373 (2010).
45. Kossin, J. P. Validating atmospheric reanalysis data using tropical cyclones as thermometers. *Bull. Am. Meteor. Soc.* **96**, 1089–1096 (2015).
46. D'Asaro, E. A. et al. Impact of typhoons on the ocean in the Pacific: ITOP. *Bull. Am. Meteor. Soc.* **95**, 1405–1418 (2014).
47. Lin, I. I. et al. A tale of two rapidly-intensifying supertyphoons: Hagibis (2019) and Haiyan (2013). *Bull. Am. Meteor. Soc.* **102**, E1645–E1664 (2021).
48. Schwalm, C. R., Glendon, S. & Duffy, P. B. RCP 8.5 tracks cumulative CO2 emissions. *Proc. Natl Acad. Sci. USA* **117**, 19656–19657 (2000).
49. Ting, M., Kossin, J. P., Camargo, S. J. & Li, C. Past and future hurricane intensity change along the U.S. east coast. *Sci. Rep.* **9**, 7795 (2019).
50. Price, J. F., Sanford, T. B. & Forristall, G. Z. Forced stage response to a moving hurricane. *J. Phys. Oceanogr.* **24**, 233–260 (1994).
51. Price, J. F. Upper ocean response to a hurricane. *J. Phys. Oceanogr.* **11**, 153–175 (1981).
52. Lin, I. I. et al. An ocean coupling potential intensity index for tropical cyclones. *Geophys. Res. Lett.* **40**, 1878–1882 (2013).
53. Jin, F.-F., Boucharel, J. & Lin, I. I. Eastern Pacific tropical cyclones intensified by El Niño delivery of subsurface ocean heat. *Nature* **516**, 82–85 (2014).
54. Knutti, R., Masson, D. & Gettelman, A. Climate model genealogy: Generation CMIP5 and how we got there. *Geophys. Res. Lett.* **40**, 1194–1199 (2013).

55. Sanderson, B., Knutti, R. & Caldwell, P. P. A representative democracy to reduce interdependency in a multimodel ensemble. *J. Clim.* **28**, 5171–5194 (2015).
56. Dunne, J. P. et al. The GFDL earth system model version 4.1 (GFDL-ESM 4.1): overall coupled model description and simulation characteristics, *J. Adv. Model. Earth Syst.* **12**, e2019MS002015 (2020).
57. Li, T. et al. Global warming shifts Pacific tropical cyclone location. *Geophys. Res. Lett.* **37**, L21804 (2010).

AUTHOR CONTRIBUTIONS
I.L. and S.C. initiate the research. I.L., C.L., C.S. conduct the analyses. I.L., S.C., J.K. interpret the results. S.C. provides the C-tracks. I.L. drafts the MS with input from S.C. and J.K.

COMPETING INTERESTS
The authors declare no competing interests.

ADDITIONAL INFORMATION
Supplementary information The online version contains supplementary material available at https://doi.org/10.1038/s41612-023-00329-y.

Correspondence and requests for materials should be addressed to I.-I. Lin.

Reprints and permission information is available at http://www.nature.com/reprints

Publisher's note Springer Nature remains neutral with regard to jurisdictional claims in published maps and institutional affiliations.